Structure–Function Tuning of Lyotropic Liquid Crystal-Carbon Nanotube Composites for Drug Delivery

ACS APPLIED NANO MATERIALS

www.acsanm.org

Article

Structure–Function Tuning of Lyotropic Liquid Crystal-Carbon Nanotube Composites for Drug Delivery

Aleksandra Benko,* Annija Stepulane, Marcel Zambrzycki, Marta Gajewska, Magdalena Ziąbka, and Martin Andersson

Cite This: *ACS Appl. Nano Mater.* 2026, 9, 6665–6678

Read Online

ACCESS | Metrics & More | Article Recommendations | Supporting Information

ABSTRACT: Incorporating carbon nanotubes (CNTs) into polymeric hydrogels significantly expands their functional capabilities in biomedical applications. By improving printability and regulating drug release, CNTs enable the 3D printing of these hydrogels into custom geometries tailored to complex wound beds. Functionalized CNTs are dispersible in solvents and have polar and nonpolar sites that can interact with the polymer, possibly affecting its structure. This study was designed to investigate this phenomenon with a photo-cross-linkable diacrylated Pluronic F127 (DA-F127) utilized as a model able to self-assemble into lyotropic liquid crystal (LLC) phases. Micellar cubic (Mic) and hexagonally ordered fibrillar (Fib) phases were mixed with two types of covalently functionalized CNTs. The structural and functional properties of the nanocomposites were investigated for potential applications: 3D-printable inks, drug-delivery scaffolds, and wound dressings. The aim was to provide a guideline for the optimal pairing of the compounds. Amide-modified CNTs performed optimally in the Fib phase, whereas oxidized CNTs were best suited for the Mic phase. Proper pairing resulted in improved printability and drug release profiles while maintaining the LLC phase ordering, whereas using CNTs in the opposite combinations disrupted the LLC order.

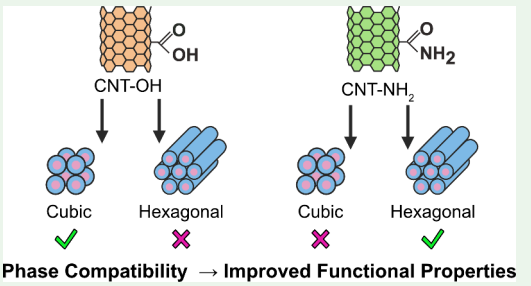

KEYWORDS: *Diacrylated Pluronic F127, carbon nanotubes, lyotropic liquid crystals, hydrogel nanocomposites, drug delivery, 3D printing*

1. INTRODUCTION

Carbon nanotubes (CNTs) exhibit a range of intriguing physicochemical properties, including good electrical and thermal conductivity, photothermal and photodynamic effects, high mechanical strength, and antibacterial and anticancer properties.[1−4] As such, CNTs are extensively studied for numerous applications, particularly in the biomedical field, for example, in biosensors, wearable electronics, drug delivery systems, and tissue engineering constructs.[2,5,6] A critical requirement for these applications is cytocompatibility, which depends strongly on specific physicochemical characteristics, such as surface chemistry, dimensions, and dispersibility. It is now well-established that short CNTs, approximately 30 nm in diameter, when chemically functionalized and dispersible in polar liquids, exhibit good cytocompatibility.[7,8]

Among various applications, CNTs have been suggested as additives for polymer matrices, where they can impart materials with their native properties.[9−12] Recently, a range of commercial and noncommercial formulations combining different hydrogels with CNTs have become available.[13,14] However, the impact of CNTs on the processability and structural properties of these materials remains largely unexplored. Importantly, effective processing of polymer−CNT nanocomposites requires properly matching the physicochemical properties of the two components. CNTs' size, dispersion, and functionalization, alongside the polymer and solvent type, all govern the interactions with the polymer chains. These factors directly influence the quality of the final product.[12,15,16] The challenge is further exacerbated in amphiphilic systems where the coexistence of polar and apolar domains, originating from the polymer, CNTs, and solvents, creates a multitude of complex interaction possibilities. Studying such materials is of great importance, as their amphiphilic character is favorable for drug delivery applications, as well as in various filtration systems, where compatibility with polar and apolar target molecules is highly desirable.[17] In these applications, CNTs can introduce new binding sites, affect the binding strength, and be used to control the release of target molecules.[2] During the processing of such nanocomposites, interfacial interactions may influence the polymer's microstructure, an aspect that must be considered in material design.[18]

This present study was designed to address key challenges in the fabrication and design of amphiphilic copolymer-amphiphilic CNT systems. We selected one of the most

Received: January 16, 2026
Revised: March 25, 2026
Accepted: March 26, 2026
Published: April 9, 2026

https://doi.org/10.1021/acsanm.6c00241
ACS Appl. Nano Mater. 2026, 9, 6665−6678

widely used amphiphilic copolymers, Pluronic F127 (PEO_{100}-PPO_{70}-PEO_{100} (poly(ethylene oxide)-poly(propylene oxide)-poly(ethylene oxide) triblock copolymer)), which has received FDA approval for use in pharmaceutical formulations, medical devices, and drug delivery systems. The PEO part of F127 is hydrophilic, while the PPO part is hydrophobic. We used functionalized CNTs in which amphiphilic properties arise from the hydrophobic graphene planes and hydrophilic functional groups. Pluronic F127 can self-assemble into various phases (e.g., micellar cubic, lamellar, hexagonal, etc.) when mixed with block-selective polar and apolar solvents, forming lyotropic liquid crystal (LLC) mesophases.[19,20] This property has been extensively studied for encapsulation and delivery of both polar and apolar drugs[21,22] as well as for forming ordered materials, including elastomeric materials and structured bone-mimetic nanocomposites.[23−25] Upon chemical modification, such as the introduction of acrylate groups, Pluronic F127 can form photo-cross-linkable hydrogels that are 3D-printable and suitable for applications such as scaffolds with designed architectures or wound dressings tailored to irregular wound beds.[26]

In this study, two Pluronic F127 oil−water systems yielding distinct micellar cubic (Mic) and hexagonally ordered fibrillar (Fib) phases were combined with two types of chemically modified multiwalled CNTs, oxidized (HO) and amidized (HNH, derived from HO), and systematically analyzed. The CNTs used herein were selected based on our previous studies,[6,27] wherein they were characterized by good dispersibility in polar liquids, cytocompatibility, and anticancer and antibacterial properties. Importantly, these features were also inherited by layers and carbon−carbon composites made from them.[11,28] Full physicochemical characterization can be found in previous publications.[6,27] Briefly, HO had roughly 16% of oxygen atoms at their surface with 30% of them double-bonded with carbon. In HNH, 12% of oxygen atoms and 2% of nitrogen atoms were recorded at the surface. Both had diameters between 10 and 50 nm and lengths between 100 and 800 nm. The two were characterized by different electron donor properties (work function of 4.84 eV (HO) and 4.57 eV (HNH)) and different values of dipole moments related to characteristic functional groups, especially in their projection in the direction perpendicular to the carbon surface (−0.02 in COOH of HO and 0.21 in $CONH_2$ of HNH). Such different polarities and electron donor properties are expected to selectively interact with different functional groups on diacrylated Pluronic F127 (DA-F127), affecting their assembly in LLCs. We expected that polar HO would be more compatible with Mic phases, which are obtained in water, while a slightly less polar HNH would be more suitable for modifying Fib phases that are made in a water−butanol system.

The main objective was to establish correlations between the materials used in the nanocomposite preparation and the resulting physicochemical and functional properties of the obtained nanocomposites. Finally, by loading polar and apolar model drugs into these systems, the influence of CNT chemistry and Pluronic F127 LLC phase structure on drug loading, distribution, and release behavior was elucidated, providing insights for the future design of multifunctional nanocomposites for biomedical applications. Current research on hydrogel−CNT nanocomposite fabrication is largely phenomenological. Existing literature frequently describes the mixture of polymers with commercially available, poorly characterized CNTs, often omitting in-depth investigations of polymer−CNT interactions or systematic analyses of varying composite ratios. Our study bridges this gap by offering a mechanistic explanation of the observed phenomena and establishing fundamental guidelines for designing novel nanocomposites.

2. MATERIALS AND METHODS

2.1. CNT Functionalization

Unmodified CNTs were supplied by NanoAmor (#1237YJS, Nanostructured & Amorphous Materials, Inc., USA). According to the producer, these CNTs are >98% pure and have outside diameters of 20−30 nm and lengths of 0.5−2 μm. These CNTs were subjected to chemical oxidation by refluxing in a 3:1 mixture of H_2SO_4 and HNO_3 as described in our previous studies.[6,27] Throughout this study, these CNTs are denoted as HO. HO was then subjected to a successive amidization, performed via EDC (1-ethyl-3-(3-(dimethylamino)propyl)carbodiimide hydrochloride) and NHS (*N*-hydroxysuccinimide) (both supplied by Merck) via EDC and NHS activated coupling of ammonia. Briefly, 300 mg of HO was dispersed in 25 mL of phosphate-buffered saline (PBS, sterile ROTICell, Carl Roth) using an ultrasonic probe (Vibra-cell, type VCX 130 from Sonics & Materials, Inc., equipped with a 6 mm probe, operating at a 30% of maximum amplitude for 2 min). EDC and NHS were each dissolved in 25 mL of PBS. The EDC solution was then added to the HO dispersion and sonicated for 30 s, followed by NHS addition and another 30 s of sonication. The as-obtained mixture was then stirred with a magnetic stirrer at 300 rpm for 3 h to allow formation of amine-reactive NHS ester. To remove reaction byproducts and unreacted compounds, the mixture was centrifuged twice, with one medium exchange to PBS, for 1 h at 15 000 rpm. Next, the activated product was dispersed in 100 mL of 40% ammonia (Avantor chemicals), sonicated for 2 min at 30% amplitude, and stirred at 300 rpm for 24 h. Finally, the CNTs were centrifuged twice with one medium exchange to 80% ethanol (centrifuge: Sigma 3-30K, 15 000 rpm, 1.5 h) and dried in a vacuum oven at 40 °C for 72 h (Vacucell Eco 55). The dried pellet was mortared and stored in a desiccator for further use.

2.2. CNT-Pluronic F127 Nanocomposite Preparation

The different CNT-Pluronic F127 nanocomposite samples were prepared based on a Pluronic F127−oil−water ternary system reported previously.[19,20,29] In this work, two distinct Pluronic F127−oil−water compositions were utilized. The samples were prepared by mixing DA-F127 copolymer powder (Acr-PEO_{100}-PPO_{70}-PEO_{100}-Acr, M_w = 12 600 g/mol, Amferia AB, Sweden) with water and butanol as the oil phase in concentrations known to form characteristic microstructures, i.e., normal (oil-in-water) micellar cubic (denoted by Mic) and normal hexagonally ordered fibrillar (denoted by Fib) (see Table 1).

For the preparation of the nanocomposites, the chemically functionalized HNH and HO were dispersed in Milli-Q water using an ultrasonic probe (2 min, 20% amplitude) and stored at 4 °C for further use. The CNT concentration in the dispersions was

Table 1. Sample Compositions of CNT-Pluronic DA-F127 Nanocomposites

Sample ID	DA-F127, wt %	Butanol, wt %	Water, wt %	CNT functionality[a]
Mic	30		70	
Mic_HNH	30		70	amidized
Mic_HO	30		70	oxidized
Fib	35	15	50	
Fib_HNH	35	15	50	amidized
Fib_HO	35	15	50	oxidized

[a]At 0.25 wt % of dry DA-F127 mass.

https://doi.org/10.1021/acsanm.6c00241
ACS Appl. Nano Mater. 2026, 9, 6665−6678

maintained at 1.75 mg/mL with the dispersion serving as a stock for further nanocomposite synthesis.

For Mic_HNH and Mic_HO samples, aliquots of each CNT stock dispersion were pipetted in plastic containers, further diluted with Milli-Q water to 1.07 mg/mL, sonicated for an additional 30 s, and cooled at 4 °C. To prepare the nanocomposite gels, 700 μL of the resulting CNT dispersions was manually mixed with 300 mg of DA-F127 copolymer powder, resulting in the formation of 1 g of 30 wt % DA-F127 nanocomposite gel. To enable polymerization, the nanocomposite gels were supplemented with a photoinitiator 2-hydroxy-4-(2-hydroxyethyl)-2-methylpropiophenone (Irgacure 2959, Sigma) at a concentration of 1 wt % with respect to the dry polymer weight. The final gel mixtures were refrigerated, followed by final homogenization via hand mixing. The CNT-free Mic reference samples were prepared in a similar manner using pure Milli-Q water instead of CNT stock dispersions.

For the Fib_HNH and Fib_HO samples, undiluted CNT stock dispersions were used. To prepare the nanocomposite gels, 500 μL of the CNT stock dispersions were manually mixed with 350 mg of DA-F127 copolymer powder and cooled at 4 °C. Subsequently, 150 mg of butanol was added to the mixture, resulting in the formation of 1 g of 35/15/50 wt % (DA-F127/butanol/water) nanocomposite gel. Additionally, 1 wt % (with respect to dry DA-F127 weight) of Irgacure 2959 was added to the mixture to enable further polymerization. The final mixtures were refrigerated, followed by homogenization via hand mixing. The CNT-free Fib reference samples were prepared in a similar manner using pure Milli-Q water instead of the CNT stock dispersions.

The final CNT concentration was remained constant in all the CNT-containing nanocomposite samples with 0.25 wt % CNTs per dry DA-F127 polymer weight.

2.3. Preparation of Gels in the Form of Thin Films and Printouts

Depending on the viscosity of the nanocomposite gel, the refrigerated gels were either directly cast between two glass slides using approximately 0.15 mm thick coverslips as spacers (Mic gels) or loaded into syringes, centrifuged at 4000 rpm for 20 min to remove trapped air bubbles, and then cast in the same manner (Fib gels). The resulting assemblies were exposed to UV light (λ = 365 nm) for 3 min per side, leading to UV-induced photopolymerization of the DA-F127 network into solid film-shaped materials.

Separately, each gel type was loaded into a syringe, centrifuged, and extruded. The extrusion was conducted using a BioX 3D printer (Cellink) equipped with a temperature-controlled pneumatic printhead set to 15 °C. A plastic 30 G tip was used, and the polymer was extruded at 60−110 kPa. Pressure, preflow, and postflow parameters were adjusted depending on the gel type, and the printing speed was set to 10 mm/s. A 10 × 10 × 0.3 mm cube with a 25% infill density of grid pattern was printed to evaluate differences in printout resolution. The printed structures were photopolymerized using UV light (λ = 365 nm) for 3 min on each side (POLBIONICA UV−vis Lamp).

2.4. Morphology of the Gels

Optical microscopy was used to visualize the distribution of CNTs in the polymer matrix before and after polymerization. A fluorescence microscope (ZEISS Axio) operated in bright-field mode was employed. Uncross-linked gel samples were smeared as a thin layer between two glass coverslips, whereas cross-linked thin films were imaged in their as-prepared state.

The morphology of the as-prepared printouts was visualized by using a Keyence digital optical microscope (VHX-900F). Diameters of the printout strands were analyzed using the microscope's software by measuring at least 12 different strands across a minimum of three different printouts, and the results are reported as mean ± standard deviation.

Scanning electron microscopy (SEM) was performed to visualize the surfaces and cross sections. Cross sections were prepared by flash-freezing the materials in liquid nitrogen followed by fracturing. All samples were mounted on aluminum SEM stubs using carbon adhesive discs (cross sections were glued to 90° angled stubs) and sputter-coated with a 6 nm carbon layer (Leica EM ACE600 High Vacuum Sputter Coater, Wetzlar). Imaging was conducted at 2−5 kV using a T1 in-lens detector on an Apreo 2S low-vacuum SEM (ThermoFisher Scientific).

Transmission electron microscopy (TEM) was used to visualize the internal morphologies of the films. TEM lamellae were prepared by using plasma-focused ion beam (PFIB) milling on a Helios 5 CXe DualBeam system (Thermo Fisher Scientific). TEM imaging was performed using an FEI Tecnai TF20 X-TWIN (FEG) microscope at an accelerating voltage of 200 kV. Bright field (BF) and high-resolution TEM imaging were used to visualize CNTs and assess their influence on the material's internal structure.

2.5. Chemical Characterization

Fourier-transform infrared spectroscopy (FTIR, Tensor 27, Bruker), operating in attenuated total reflectance mode (ATR, Quest Diamond accessory, Specac), was used to identify changes in the chemical composition of the samples as well as to detect any possible chemical interactions between the CNTs and the polymer matrix. A clean ATR crystal was used as a background. For each sample, a total of 64 scans were recorded and averaged at a spectral resolution of 4 cm^{-1}. After the measurements, the spectra were smoothed, corrected for background noise, and normalized in the 3963−3060 cm^{-1} region using OPUS v7.2 software.

2.6. Thermal Analysis

Simultaneous thermal analysis (STA, 449 F3 Jupiter, Netzsch) was employed to investigate the effect of different LLC phases and the presence of the CNTs on the thermal properties of the as-obtained samples. Thermogravimetry (TG) provides information about the overall thermal stability, which may reveal differences in the structural organization of the LLCs. Meanwhile, differential scanning calorimetry (DSC) was used to analyze changes in heat flow during heating, thereby identifying thermal transitions and their associated energy changes. Approximately 8 mg of each sample was loaded separately into an alumina crucible without a lid, with an empty crucible serving as a reference. The samples were heated at a rate of 10 °C/min from 40 to 800 °C under the protective flow of nitrogen (50 mL/min). Data were corrected against a blank run conducted under the same experimental conditions. After measurements, TG and DSC curves were analyzed using Proteus 6.1 software.

2.7. Structural Characterization

Small-angle X-ray scattering (SAXS) measurements were conducted using a Mat: Nordic (SAXSLAB) instrument equipped with a Rigaku MicroMax-003+ Cu-radiation source and a Pilatus 300 K detector over a q range of 0.007−0.306 $Å^{-1}$ and with an X-ray wavelength of λ = 1.54 Å. Uncross-linked Mic and Fib gel samples were measured in 2 mm glass capillaries and in sandwich cells with Kapton windows, respectively, while the cross-linked nanocomposite films were placed on an ambient sample holder plate and secured with tape (Scotch Magic tape, 3M). All SAXS measurements were performed under a vacuum with an X-ray exposure time of 1 h for the uncross-linked gel samples and 20 min for the cross-linked films.

SAXS peaks were fitted to a Gaussian function to determine the peak position at the maximum intensity. The average lattice parameter d was calculated using the following equation:

$$d = \frac{2\pi}{q}$$

where q is the recorded SAXS peak position at maximum intensity.

2.8. Swelling Experiments

Swelling experiments were performed to assess the cross-linked samples' capacity to take up water, a property relevant for drug encapsulation and delivery studies as well as for electrical conductivity measurements. Circular discs with a diameter of 8 mm were punched out from the as-prepared nanocomposite sample films (including the reference Mic and Fib samples), using a biopsy punch, and air-dried at 37 °C until reaching constant weight. The samples were then

https://doi.org/10.1021/acsanm.6c00241
ACS Appl. Nano Mater. 2026, 9, 6665−6678

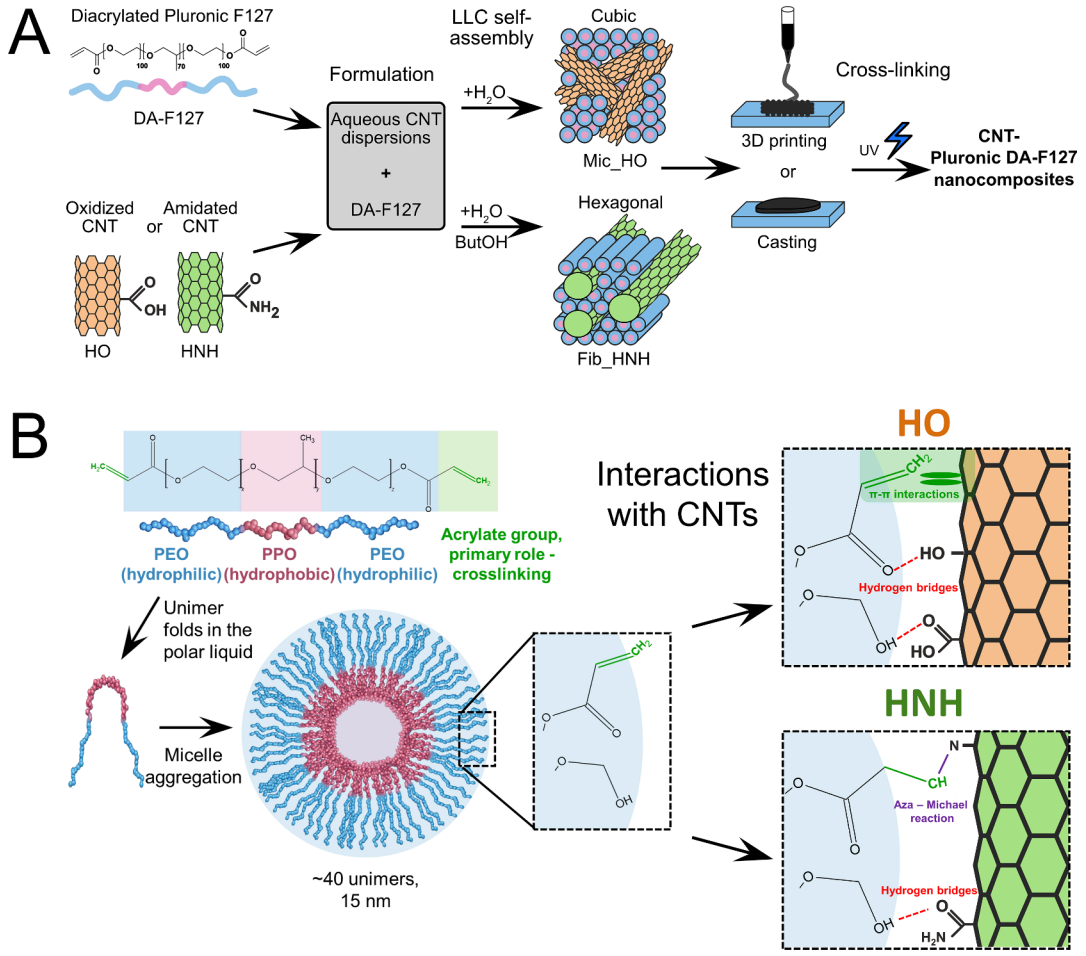

Figure 1. (A) Schematic representation of the proposed CNT-Pluronic F127 nanocomposite sample production process based on micellar cubic (Mic) and hexagonally ordered fibrillar (Fib) Pluronic F127 phases with oxidized (HO) and amidized (HNH) carbon nanotubes incorporated in the nanocomposite structure. (B) Schematic representation of how the micelles are formed in the liquid and some possible chemical interactions that may be occurring between the HO/HNH and the polymer. Not all prepared materials and not all possible interactions are depicted.

immersed in Milli-Q water and allowed to swell with their weight monitored every 15 min until no changes were observed. The sample swelling ratio was calculated according to the following equation:

$$\%S_w = \frac{w_t - w_0}{w_0} \times 100$$

where w_t is the swollen sample weight at a given time point and w_0 is the dry sample weight. Two independent sets of six samples were measured for each sample type. The obtained results are presented as mean ± standard deviations, expressed as a function of time.

2.9. Electrical Conductivity

The conductivity of the samples was determined by using sheet resistance measurements with a four-point-probe system from Ossila. A target current of 0.1 μA and a maximum voltage of 1 V were applied. Each sample type was tested in triplicate, and the results are reported as the mean ± standard deviation. For conductivity calculations, the thickness of the materials was measured by using a micrometer screw with at least three random points taken on each sample and averaged.

2.10. Drug Delivery from the Materials

Nanocomposite samples were prepared and evaluated for their ability to encapsulate and release therapeutic drugs with varying chemical polarities. The different sample compositions were mixed, as described in Section 2.2. The resulting gels were cast between two glass slides using 0.6 mm-thick aluminum foils as spacers and exposed to UV light (λ = 365 nm) for 4 min on each side, forming solid films. Circular sample discs, 8 mm in diameter, were then punched out of the films using a biopsy punch.

To remove any loosely bound polymer or CNTs, the discs were washed for 72 h using Milli-Q water and acetone for the Mic and Fib samples, respectively, with the washing medium changed daily. After being washed, the samples were air-dried at 37 °C for 24 h and subsequently loaded with the model drugs. Vancomycin (VCM), an antibiotic, was selected as the polar model drug, while ibuprofen (IBU), a nonsteroidal anti-inflammatory drug, was used as the nonpolar model drug. The dried sample discs were immersed for 48 h in 1 wt % solutions of VCM in Milli-Q water or IBU in acetone, respectively.

After drug loading, the samples were washed with either acetone or water, depending on the drug's polarity, and then air-dried for 24 h at 37 °C. The dry, drug-loaded samples were immersed in 5 mL of either Milli-Q water (for VCM) or a 1 wt % sodium dodecyl sulfate (SDS) solution (for IBU) as the drug release medium. To monitor drug release, 2 mL aliquots of the release medium were regularly collected and replaced with fresh solvent to maintain constant volume. Drug release was quantified using a UV−vis spectrophotometer (Multiskan GO, Thermo Fisher Scientific) by measuring absorbance at λ = 280 nm for VCM and λ = 272 nm for IBU. The drug release was quantified using previously constructed standard curves, and the results were expressed as the mass of drug released per unit. To account for periodic sampling and medium replacement, cumulative drug release at time t was calculated as

https://doi.org/10.1021/acsanm.6c00241
ACS Appl. Nano Mater. 2026, 9, 6665−6678

$$M_t = C_t \cdot V_0 + V_s \sum_{i=1}^{t-1} C_i$$

where

C_t − concentration measured at time point t,
V_0 − total release volume,
V_s − sampled volume,
C_i − concentration measured at time point i.

Cumulative release for each specimen was normalized to its dry sample mass and presented as mean cumulative drug release per gram of dry sample ± standard deviations from three replicates, plotted as a function of time.

3. RESULTS AND DISCUSSION

Figure 1A provides an illustrative overview of the preparation of CNT_-hydrogel nanocomposites comprising micellar cubic (Mic) or hexagonally ordered fibrillar (Fib) Pluronic F127 mesophases as the hydrogel matrix material, together with oxidized (HO) or amidized (HNH) CNTs as the nanofiller. The combination of these components results in example compositions such as Mic_HO and Fib_HNH CNT-Pluronic DA-F127 nanocomposites with additional compositions not depicted in the image. Some possible chemical interactions that may be happening between DA-F127 and the CNTs are depicted in Figure 1B. In polar solvents, the DA-F127 molecule will adopt a conformation that maximizes interactions of the PEO units with the solvent, while minimizing it for the PPO. This results in folding. At a critical temperature and concentration, these U-shaped molecules will aggregate into micelles. Depending on the solvent used, temperature, and concentrations, micelles will then self-assemble into LLCs. When there is just water in the system, they will create a micellar cubic phase. In the presence of ButOH, they will create a fibrillar hexagonal phase wherein continuous hydrophobic PPO cores will store butanol. In both LLCs, C═O, C−OH, and acrylate groups will be exposed. In the presence of CNTs, these groups are expected to interact with their functional groups. OH and COOH of HO are prone to create hydrogen bridges with the C═O and C−OH groups of DA-F127. Amine and amide groups of HNH can also form hydrogen bridges, but there is also a possibility of undergoing some Aza-Michael reactions, creating new, covalent bonds between the nitrogen atoms and the acrylate groups.[30] This might partially consume groups that are responsible for light-triggered cross-linking. Because the overall amount of nitrogen atoms is 2% at. and the CNTs were added at a 0.25% concentration, we do not expect this to be observable. In the Fib phase, HNHs with their positive dipole moment can orient themselves along the fibril axis (Figure 1). The graphitic planes of both CNT types facilitate $\pi-\pi$ stacking with the C═C bonds found in the acrylate groups.

3.1. Morphology of the Nanocomposites

To evaluate the effects of incorporating different CNT types on the morphology of the nanocomposite samples, both uncross-linked thin gel layers and their corresponding cross-linked thin films were imaged using optical microscopy. The optical microscopy images (Figure 2) revealed variations in CNT distribution within the polymer matrix. In the uncross-linked gel state (Figure 2A), all samples exhibited an overall homogeneous CNT distribution; however, some degree of aggregation on the microscale was observed, indicating CNT clusters despite the chemical functionalization. Among the samples, Fib_HNH gel exhibited the most homogeneous

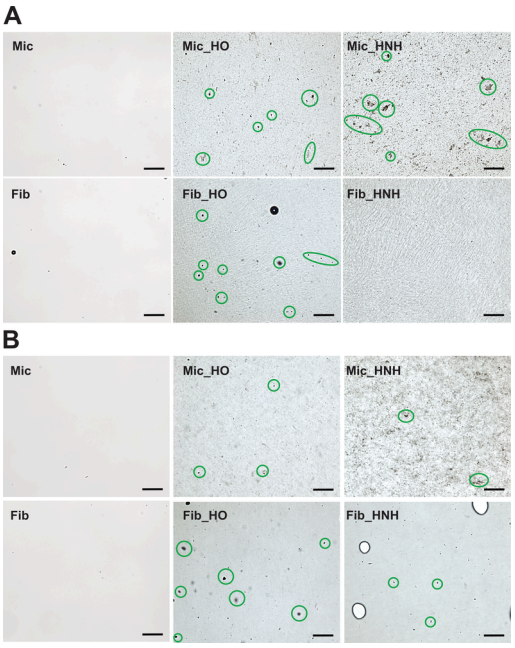

Figure 2. Optical microscopy images of the uncross-linked gel samples (A) and the cross-linked nanocomposite thin films (B). CNT aggregates highlighted with green circles. Scale bar, 100 μm.

structure, characterized by the absence of detectable CNT aggregates. It also exhibited a distinct streak-like pattern when interacting with light visible in the background. A similar pattern was observed in the Fib_HO gel. In contrast, the Mic_HNH gel demonstrated the poorest CNT distribution with aggregates ranging in size from 10 to 30 μm. The Mic_HO and Fib_HO samples displayed intermediate levels of CNT distribution. In these samples, the presence of a grayish color combined with the presence of observable aggregates indicates that there are two populations of CNTs within these nanocomposites: some evenly dispersed within the matrix and some forming agglomerates. These agglomerates are likely enveloped by DA-F127, potentially influencing the structural arrangement of the nanocomposite.

Upon polymerization (Figure 2B), only minor changes in the CNT distribution were observed. Fib_HNH maintained the most homogeneous CNT pattern with minimal aggregation, whereas Mic_HNH displayed significantly more microscale aggregates. The streak-like optical patterns observed in the Fib_HO and Fib_HNH gels disappeared after cross-linking. Overall, these results suggest that UV-induced polymerization does not bring any significant CNT aggregation and largely preserves the prepolymerization. However, CNT surface chemistry plays a key role in their distribution within the DA-F127, which is greatly affected by the solvents used in sample preparation. In the polar-only Mic composition, the less polar HNHs are forced together and form aggregates, likely wrapped in DA-F127, causing localized distortion of the structural arrangement. In contrast, when the apolar butanol solvent is present in the mixture, as in the Fib sample, HNHs disperse well, suggesting that individual CNTs interact favorably with DA-F127, which then interact with a compatible and highly organized network.

The microstructure of the as-prepared nanocomposite samples, along with the Mic and Fib reference samples, was examined by using SEM. Except for Fib_HO, the introduction

https://doi.org/10.1021/acsanm.6c00241
ACS Appl. Nano Mater. 2026, 9, 6665−6678

of CNTs contributed to a slightly smoother surface topography (Figure 3). The Mic_HO and Fib_HNH samples exhibited

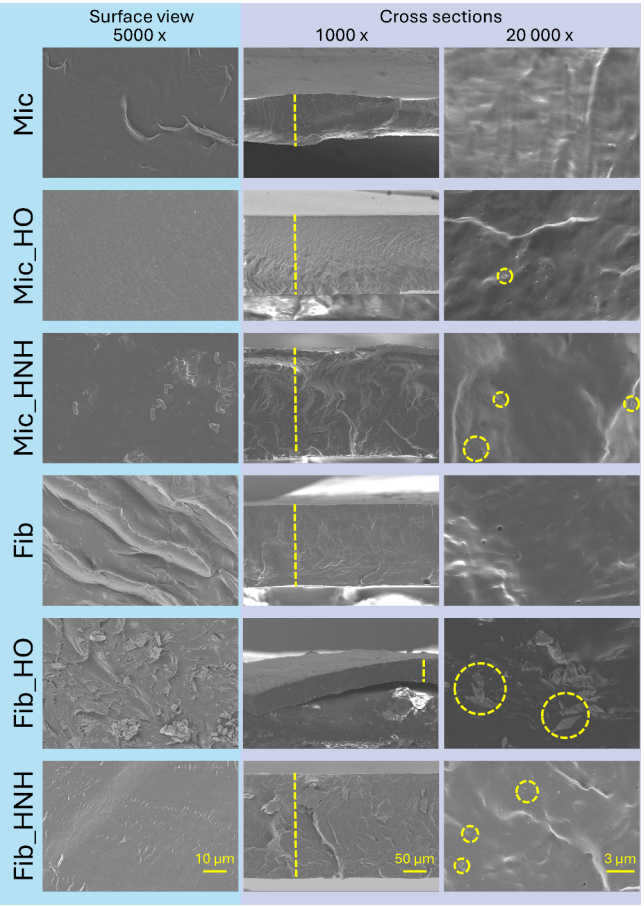

Figure 3. SEM micrographs of the nanocomposite surfaces and cross sections (denoted with a yellow dashed line). The agglomerates are marked with yellow circles.

the most pronounced surface smoothening effect, suggesting that the introduction of functionalized CNTs into the DA-F127 matrix enhances gel flowability before polymerization, yielding a more even surface microtopography after cross-linking. The data further suggest that different CNTs' surface chemistries are compatible with different DA-F127 phases: HOs appear more homogeneously distributed in Mic, whereas HNHs appear to be better dispersed in Fib. This suggests that HO is more compatible with water, while HNH is more compatible with butanol. We suggest that when CNTs–DA-F127 phase compatibility is suboptimal (as evidenced by agglomerates visible in the optical microscopy images in Figure 2), microscale features appear on the surface (evidenced by SEM in Mic_HNH and Fib_HO). In Mic_HNH, these features are smooth-edged and rod-shaped structures approximately 5 μm in size, protruding from the surface. This may suggest that, in the Mic phase, HNH agglomerates were encapsulated by amorphous, i.e., not structurally organized, DA-F127. In contrast, Fib_HO exhibits sharp, crystalline-like protrusions between 1 and 20 μm in size. This suggests that, in the presence of butanol, HO may induce structural organization of DA-F127, probably surrounding the CNT agglomerates. It is possible that this might contribute to local changes in the structural organization of DA-F127 with well-organized domains in the vicinity of HO and possibly amorphous parts further away from these CNTs, as evidenced by increased runniness of the Fib_HO solution (Figure S1, digital images of the tilted vials containing the gels). This effect may be attributed to CNTs' surface chemistry as well as their structure. It may also be governed by the presence of charged chemical species, which can affect LLC formation in a manner similar to salts.[31]

Upon fracturing the samples, the homogeneous material structure was retained throughout the bulk with no observable microphase separation, as can be seen in the sample cross sections in Figure 3 and Figure S2 (high magnification SEM images of the cross sections). Upon closer inspection, Mic_HO, Mic_HNH, Fib_HO, and Fib_HNH revealed discrete features protruding from the cross-section (circled in yellow), most likely corresponding to the CNTs. At higher magnifications, the features in Fib_HO were found to have diameters above 1 μm and displayed a lamellar structure with sharp edges, similar to the features observed on the surface of this sample. Meanwhile, individual CNTs were visible in Fib_HNH, Mic_HO, and Mic_HNH. These observations suggest that, in Fib_HO, the CNTs become wrapped with DA-F127, likely attracting hydrophilic PEO blocks and slightly distorting the overall structural organization, most probably enhancing the degree of structural ordering in the CNTs' vicinity. This effect may result from the interplay of repulsive and attractive interactions between the highly oxidized and polar CNTs and the polar and apolar solvents used in Fib production (water and butanol, respectively). The effect may be further enhanced by butanol, which swells the hydrophobic domains in the system, forcing the polar components closer together. Meanwhile, in Fib_HNH, the CNTs remain separated and are not enveloped by DA-F127. This is likely due to the different and less polar surface chemistries of these CNTs.

Thin lamellae prepared by PFIB and observed by TEM provided additional information about the microstructure of the samples (Figure 4). In all of the foils, cage-like structures were observed with their edges showing preferential redeposition of sputtered material (primarily wolfram from the protective layer). This effect was most evident in the Mic sample, whereas the plane edges were least evident in Fib_HO. This may reflect differences in the structural orientation of the LLCs, indicating that Fib_HO is characterized by lower long-range ordering. Notably, this sample was also the most fragile and prone to overheating, and cutting thin slices for TEM observation was particularly challenging. As already mentioned, the viscosity of the HO-modified DA-F127 solution in butanol was also visibly affected, supporting the hypothesis that oxidized CNTs influence the structural organization of DA-F127 (Figure S1, digital images of the tilted vials containing the gels). However, the structural distortion appears to be relatively minor as it was not detected in the SAXS analysis (Section 3.4). Across all samples, a population of CNTs was found to be well dispersed in the matrix with additional CNTs forming agglomerates, consistent with the observations from optical microscopy and SEM (Figure 2 and Figure 3). The size and number of agglomerates appear to be the largest in Fib_HO, corroborating the SEM cross-sectional results (Figure 3), where large protruding features were observed for this sample. Among all samples, Fib_HNH appears to have the most uniform CNT dispersion, indicating strong chemical

https://doi.org/10.1021/acsanm.6c00241
ACS Appl. Nano Mater. 2026, 9, 6665–6678

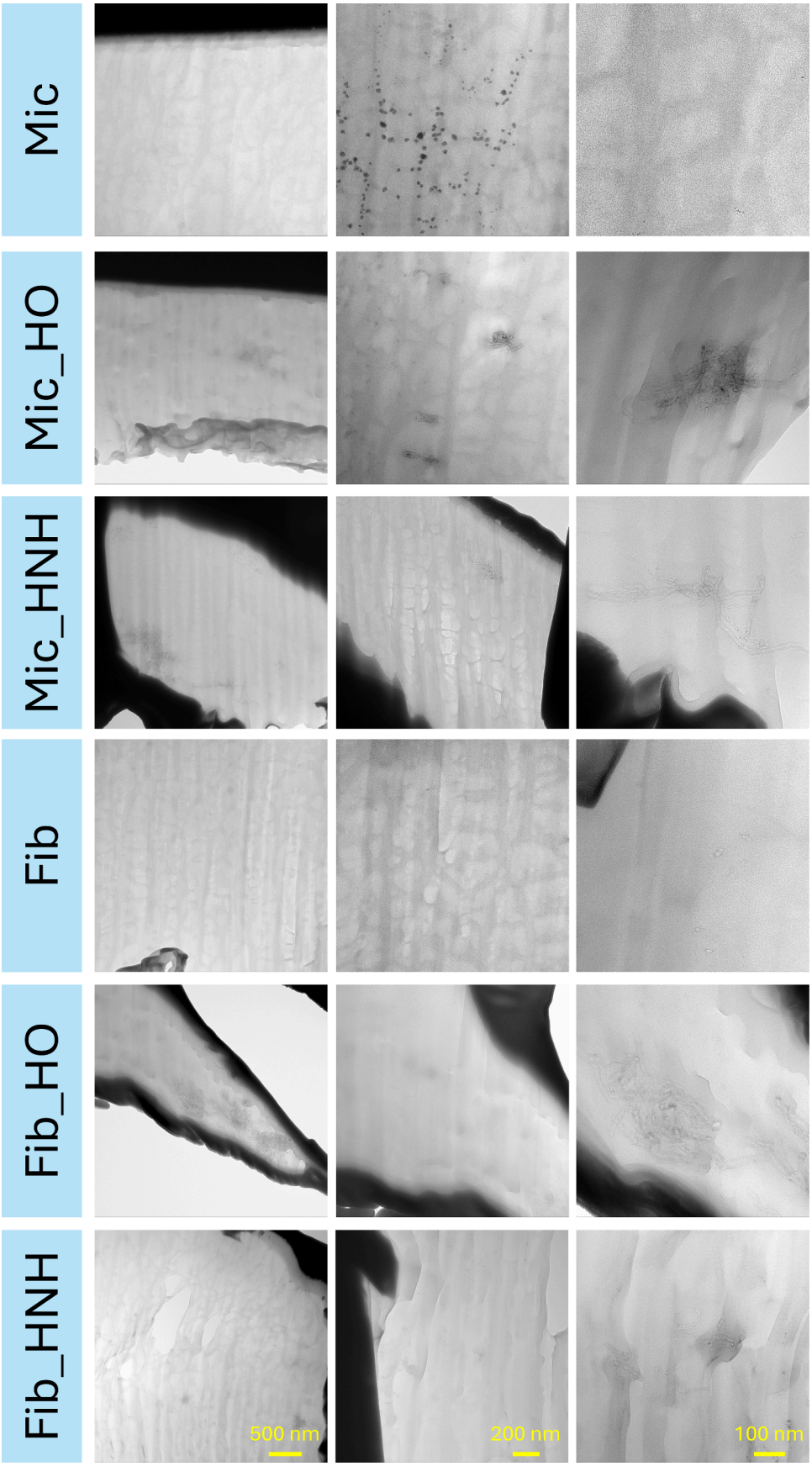

Figure 4. TEM micrographs of thin lamellae cut out from the cross-linked nanocomposites.

https://doi.org/10.1021/acsanm.6c00241
ACS Appl. Nano Mater. 2026, 9, 6665−6678

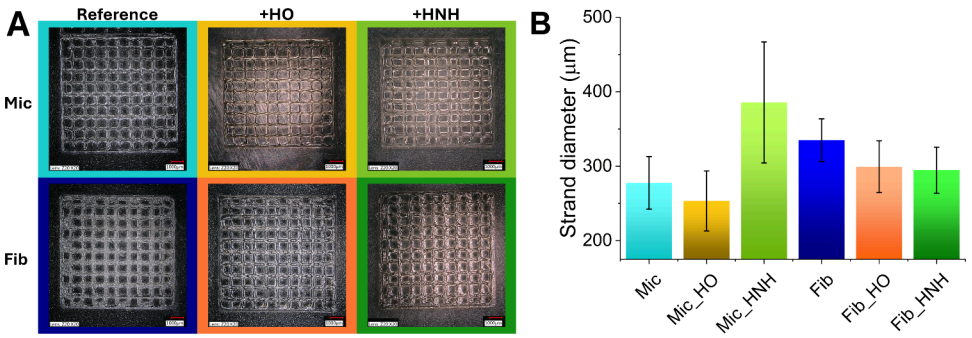

Figure 5. 3D printed scaffolds, as observed via optical microscopy (A) and the corresponding mean strand diameter, as measured from the images (B).

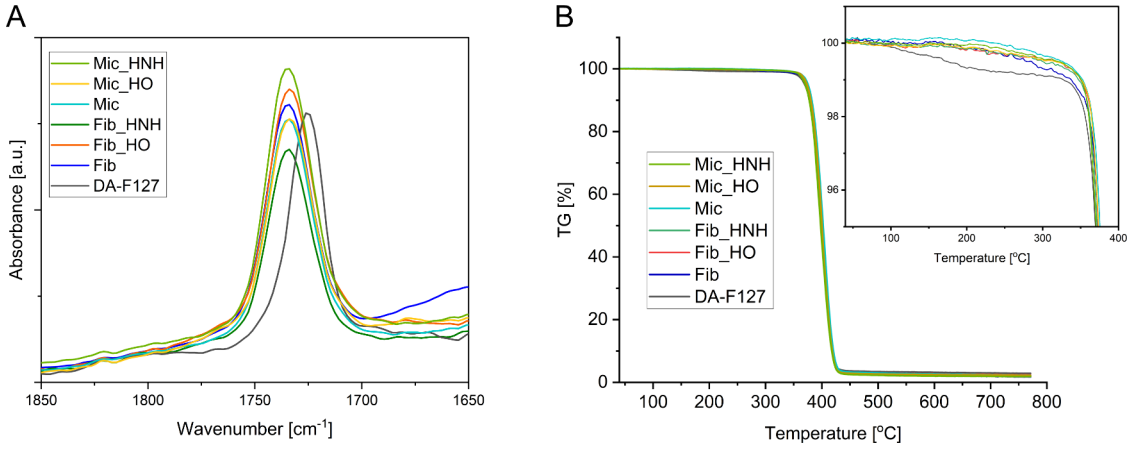

Figure 6. (A) FTIR spectra of the nanocomposite samples, reference Mic and Fib samples, and pure DA-F127 copolymer powder narrowed down to the C═O attributed bands, which are affected by cross-linking and the presence of CNTs. (B) TG curves of the tested samples are presented in the full measurement region with an inset showing a maximized section up to 400 °C to better illustrate differences in thermal stability.

compatibility between the polymer and the amide functionalized CNTs in the butanol−water environment.

The printability of the nanocomposite gels was evaluated using extrusion-based 3D printing with representative printouts and average strand diameters given in Figure 5A,B, respectively. The presence of CNTs had a significant impact on both printing resolution and shape fidelity (noting that strand widening can be caused by the top layer compressing on those below). Except for Mic_HNH, CNTs improved the printing resolution in all samples, enabling thinner strands to be extruded through a 150 μm wide tip. The highest resolution was achieved with Mic_HO (250 μm), where a self-lubricating effect was observed during printing, evidenced by the lower extrusion pressure required. Shape fidelity was also the highest with lower layers maintaining their shape even when compressed by the top layer. This is evidenced by thin and tall strands, as shown in Figure S3 (three-dimensional reconstructions of the gel printouts). In contrast, Mic_HNH exhibited the poorest resolution with strand diameters averaging approximately 400 μm. This reduced printability is likely due to the presence of agglomerates as well as poor homogeneity of the gel. It may also originate from the different viscosity and lower shape stability of this gel, as can be seen in Figure S1 and Figure S3. In the Fib formulations, both types of CNTs caused a similar reduction in strand diameter (from around 335 μm to around 299 μm). In Fib samples, shape fidelity was also improved by the presence of CNTs; however, Fib_HO appeared more flattened than Fib_HNH (Figure S3), likely due to the lower viscosity of the Fib_HO gel.

3.2. Chemical Characterization

The FTIR spectra of all nanocomposite samples, offset and presented in two regions with the DA-F127 characteristic bands, are given in Figure S4 (FTIR-ATR spectra of the cross-linked nanocomposites, presented in full range (A) and narrowed to characteristic bands (B, C, and D)). All spectra exhibit features typical of DA-F127,[32] with subtle changes induced both by the CNTs and the crystalline phase. To better visualize these differences, the spectra were superimposed and the images were narrowed down to bands that show the most significant alterations (Figure 6A) with additional details provided in the Supporting Information (Figure S4 and Table S1). DA-F127 consists of PPO blocks, surrounded by PEO blocks, essentially built of repeating C−O−C, CH_2−CH_2, and CH_2−CH_3 units. The acrylate side groups introduce ester linkages and CH═CH_2 bonds. During photoinitiated polymerization, the acrylate CH═CH_2 double bond breaks, generating a reactive moiety, which can bond to another acrylate group, thereby forming a cross-linked network. When CNTs are introduced into the mixture, they can form: (1) apolar interactions and (2) polar interactions with the polymer. Apolar interactions will occur between delocalized π bonds in aromatic rings of CNTs and, most likely, CH_3 of PPO and CH═CH_2 of acrylate. Polar interactions will involve CNT functional groups (e.g., HO, C═O, CONH) and carbonyl/C−O−C of DA-F127.

https://doi.org/10.1021/acsanm.6c00241
ACS Appl. Nano Mater. 2026, 9, 6665−6678

The bands between 3000 and 2650 cm^{-1} (Figure S4B) are attributed to the stretching vibrations of saturated C−H bonds. In all samples, cross-linking causes a shift of the 2881 cm^{-1} band toward lower wavenumbers (to 2877 cm^{-1}), indicating that cross-linking alters the chemical environment of the C−H bonds.[33] This is possibly due to bond weakening (e.g., by hydrogen bridge formation) or physical restriction of vibrations due to denser packing of the polymer chains upon cross-linking. To analyze changes introduced upon cross-linking and the presence of CNTs, absolute intensities of the bands attributed to the functional groups were divided by the absolute intensity of the C−H attributed band at 2881 cm^{-1}/2877 cm^{-1} (Supporting Information, Table S2).

The band at 1725 cm^{-1} in the uncross-linked sample and at 1734 cm^{-1} in the cross-linked samples (Figure 6) is attributed to ester C═O stretching in acrylate groups. A shift toward higher wavenumbers upon cross-linking indicates an increased strain or conjugation occurring at the oxygen in the C−O−C ester moiety. This is likely due to light-induced cleavage of the CH_2═CH bond, followed by conjugation and cross-linking with another acrylate group, introducing additional strain to the polymer structure. Additionally, new hydrogen bonds may form between the oxygen atoms and the hydrogen of the newly attached molecules, which also may contribute to this shift. In relation to the C−H band intensity, the C═O ratio is increased in all the samples except for Fib_HNH with the largest changes observed in Mic_HNH and Fib_HO, i.e., the ones with the lowest microstructural homogeneity. This suggests that the band intensity reflects the structural arrangement and cross-linking efficiency in DA-F127. It appears that the structural arrangement of DA-F127, which varies depending on the solvents used in its processing, results in different interactions between the CNTs and C═O groups. In water (Mic sample), HNH increases the number of freely vibrating C═O bonds (increased intensity ratio), while the same is reduced in the butanol/water system (Fib sample, reduced ratio). HNH likely interacts more strongly with C═O in the presence of butanol, reducing CNT−CNT interactions and leading to improved HNH dispersion (as seen in Figure 2). Meanwhile, HNH in Mic and HO in Fib appear not to interact with the C═O groups of DA-F127 and may even reduce the level of its interaction with other DA-F127 molecules, as manifested by an increased intensity ratio.

HO and HNH also cause some alterations in the ratios of C−C−O, O−C−O, and C−O−C with HO mostly increasing the ratios in Fib, while HNH decreases them in Mic.[34,35] All of the results indicate that CNTs may influence the structural arrangement of the LLCs tested in this study.

3.3. Thermal Analysis

Thermogravimetric (TG) curves of the nanocomposite samples are presented in Figure 6B. Overall, no significant differences in the thermal stability were observed. The cross-linking slightly increased the temperature at which the first step of thermal decomposition occurred and reduced the mass loss rate. The unmodified Fib sample displayed a slightly lower thermal stability compared with Mic and with all nanocomposites. By comparing the TG curves of the nanocomposites with the DA-F127 powder, we observe that the thermal stability is mostly governed by the polymers' chemical structure (PEO and PPO chains) with only small alterations introduced by the LLC and cross-linking. Differences in the short-range structural organization introduced by the small amount of CNTs could not be observed. Hence, any possible effect is too minute to be recognized by the TG curves.

Full range DSC curves are presented in Figure S5 (DSC curves of cross-linked nanocomposites), showing observable differences in thermal behavior across all the different samples. To better visualize these changes, the curves are presented in two regions with Mic and Fib samples grouped with their corresponding nanocomposites (Figure 7). For all samples, the

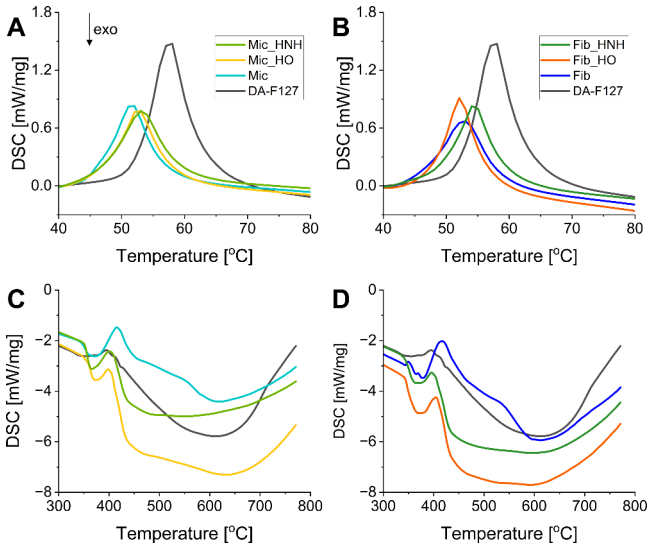

Figure 7. DSC plots of micellar cubic (A, C) and hexagonally ordered fibrillar (B, D) CNT-Pluronic F127 nanocomposites presented for two different temperature regions, including the pure DA-F127 copolymer powder.

first endothermic event is probably due to evaporation of physiosorbed water or possibly related to a glass transition accompanied by an enthalpic relaxation peak.[36]

The onset temperature of the endothermic peak was the highest for the pure DA-F127 copolymer powder sample, and accordingly, the greatest amount of energy was released in that case. In the Mic samples (Figure 7A), the presence of CNTs caused a slight shift of the onset toward higher temperatures and slightly lower energy release. In the Fib samples (Figure 7B), the presence of CNTs also increased the onset temperature toward higher values, but this time with more energy released with the highest values observed for HNH. This is likely due to the better dispersion of HNH, which provides a larger surface area of CNTs for potential chemical interactions with DA-F127 and water. Hence, more energy is needed for water evaporation.

Above 300 °C, two additional thermal effects appear in both sample types (Figure 7C,D). The first one, with an onset around 344 °C, is exothermic, whereas the second one, with an onset around 370 °C, is endothermic. Because no studies have examined Pluronic F127 or its nanocomposites at such high temperatures, we can propose only hypotheses regarding these transitions. The exothermic peak may arise from oxidation, while the endothermic peak is likely associated with melting, followed by a complete thermal decomposition of the samples.[37,38] Cross-linking appears to induce the first peak. Regardless of the LLC phase, thermal decomposition is less severe in the presence of CNTs, with reduced energy released over a shorter time frame. The peaks also become sharper, especially in the Mic samples. All these observations are likely

https://doi.org/10.1021/acsanm.6c00241
ACS Appl. Nano Mater. 2026, 9, 6665−6678

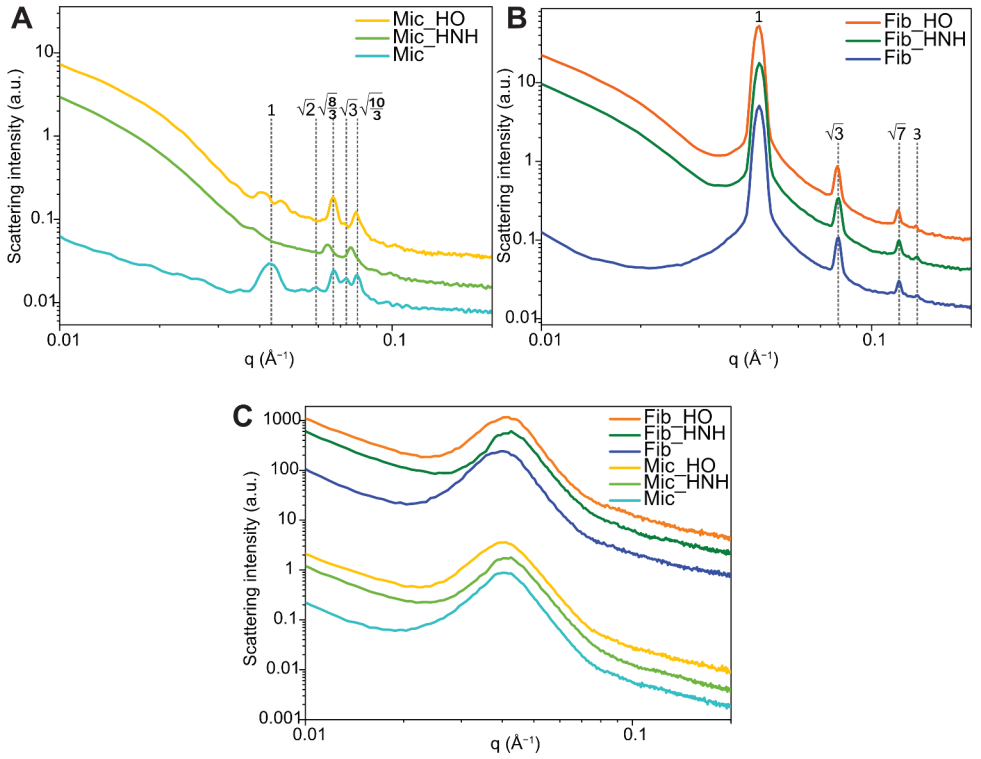

Figure 8. Recorded SAXS patterns of the uncross-linked micellar cubic (A) and hexagonally ordered fibrillar (B) CNT-Pluronic F127 nanocomposite gels. Recorded SAXS pattern of the cross-linked micellar cubic and hexagonally ordered fibrillar CNT-Pluronic F127 nanocomposites (C). Dashed lines indicate the peak positions used to index Mic samples as normal micellar cubic and Fib samples as normal hexagonal phases.

due to the improved thermal conductivity in the CNT-modified materials, so the materials are more homogeneously heated. Changes in structural arrangement may also contribute, as materials with higher structural homogeneity tend to exhibit sharper thermal events.

3.4. Structural Analysis

Mic and Fib CNT-Pluronic F127 nanocomposites were characterized with SAXS in their uncross-linked state (Figure 8A,B) and as solid films after UV polymerization (Figure 8C). The introduction of CNTs into both Mic and Fib samples before polymerization resulted in a subsequent increase of the background scattering intensity of the SAXS signal in the low q region for both HO and HNH CNT-containing samples. This behavior is typical of CNT SAXS patterns at small angles due to inherent properties of the CNTs, such as high aspect ratio and tendency to form large-scale aggregates or bundles, giving rise to increased scattering. In contrast, the uncross-linked CNT-free reference samples (Mic and Fib) did not exhibit this scattering behavior.

The reference uncross-linked Mic sample displayed five characteristic peaks at $q \approx 0.043$, 0.059, 0.067, 0.074, and 0.079 Å^{-1} (see Supporting Information Table S2 for peak positions) corresponding to a relative ratio of $1:\sqrt{2}:\sqrt{8/3}:\sqrt{3}:\sqrt{10/3}$. The first peak was the most intense, consistent with the SAXS pattern of the Pluronic F127 micellar cubic LLC phase, while slight peak broadening indicates a distribution of micellar sizes.[19,29] The observed higher-order reflections approximately follow ratios consistent with cubic ordering. In particular, the first peak at $q \approx 0.043$ Å^{-1} can be attributed to the (111) plane, while the peaks at $q \approx 0.060$ and 0.074 Å^{-1} can be tentatively assigned to the (211) and (220) reflections, respectively, in agreement with previous reports on DA-F127 systems.[19,20] In the Mic_HO sample, the first peak shifts to $q \approx 0.040$ Å^{-1} and an additional reflection appears at $q \approx 0.046$ Å^{-1}, while reflections at $q \approx 0.066$ and 0.078 Å^{-1} are retained. The feature at 0.046 Å^{-1} corresponds closely to the expected position of the (200) reflection of a cubic micellar lattice when that of (111) is ≈0.040 Å^{-1} ($q_{200}/q_{111} = 2/\sqrt{3} \approx 1.155$). This behavior is consistent with lattice expansion and increased intermicellar spacing upon incorporation of HO CNTs, rather than the formation of a new phase. In contrast, the uncross-linked Mic_HNH sample shows a further shift of the primary peak to lower $q \approx 0.038$ Å^{-1} with only two weak higher-order reflections at $q \approx 0.064$ and 0.075 Å^{-1}. The reduced number and intensity of higher-order peaks indicate a significant decrease in the long-range order. Overall, these results suggest that HO-functionalized CNTs moderately perturb the micellar cubic structure, whereas HNH-functionalized CNTs induce stronger structural disruption, potentially altering the lattice symmetry and partially disrupting the cubic arrangement.

The SAXS pattern of the uncross-linked hexagonally ordered fibrillar samples before polymerization (see Figure 8B) was indexed to a hexagonal lattice with reflections at $q \approx 0.046$, 0.079, 0.121, and 0.138 Å^{-1} corresponding to relative positions of $1:\sqrt{3}:\sqrt{7}:3$. These peaks can be assigned to the (100), (110), (210), and (300) reflections, respectively, confirming the formation of a hexagonal mesophase.[19,20] The absence of a clearly resolved (200) reflection at $2q$ is attributed to its low intensity or peak broadening. Similar behavior has been reported previously for Pluronic F127-based hexagonal LLC systems.[25] The introduction of CNTs led to an increase in background scattering intensity at lower q relative to the Fib

https://doi.org/10.1021/acsanm.6c00241
ACS Appl. Nano Mater. 2026, 9, 6665−6678

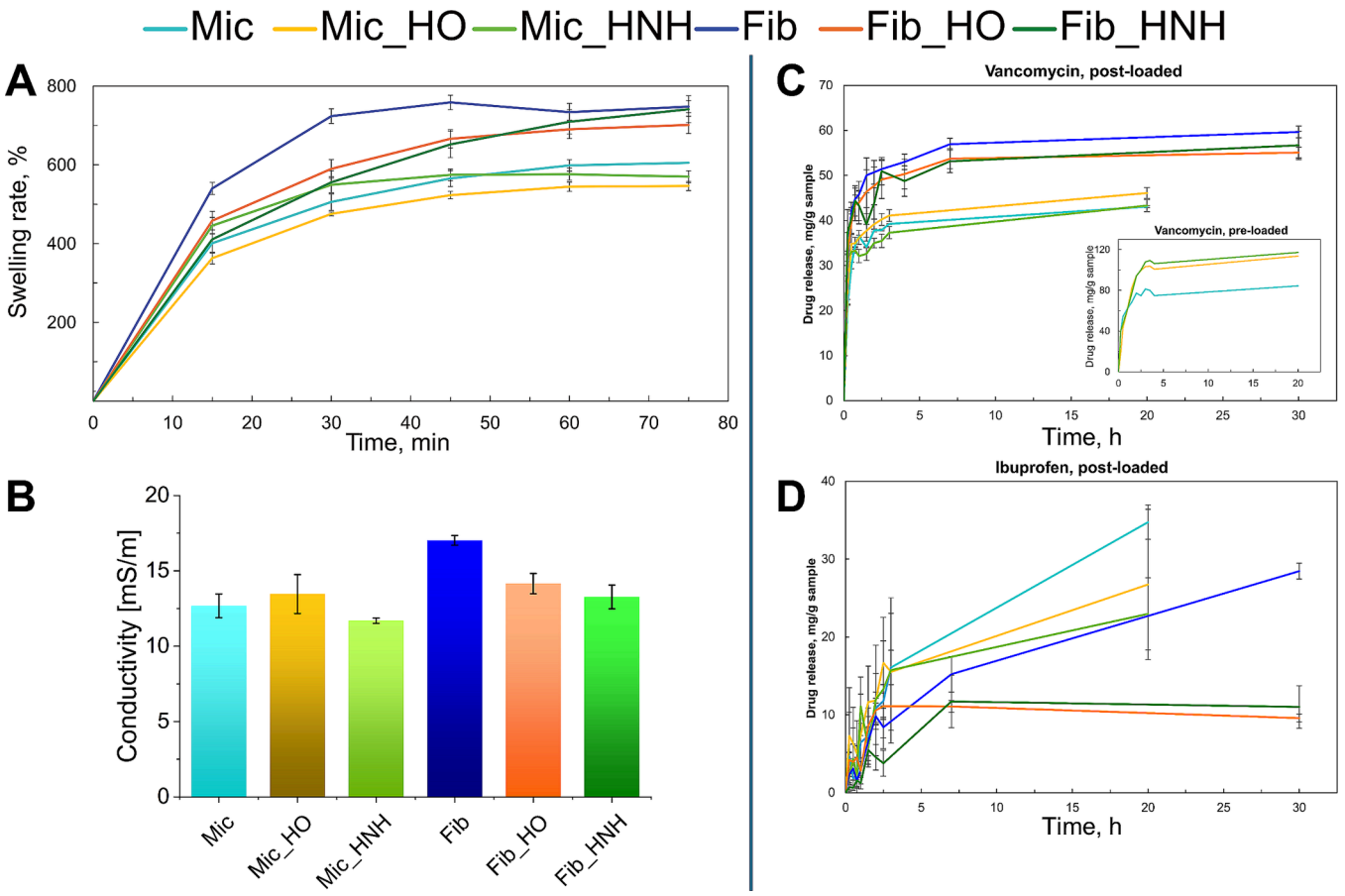

Figure 9. Swelling degree in water (A) and the electrical conductivity (B) as identified via 4-point probe measurements for the micellar cubic and hexagonally ordered fibrillar CNT-Pluronic F127 nanocomposites. Drug release profiles of vancomycin (C) and ibuprofen (D) from micellar cubic and hexagonally ordered fibrillar CNT-Pluronic F127 nanocomposites prepared via postloading conditions. Inset C shows micellar cubic samples preloaded with vancomycin exhibiting higher drug release compared to postloaded counterparts. Drug release data are normalized to dry sample mass.

reference sample without other significant changes in the diffraction peak positions.

Upon polymerization of the Mic and Fib nanocomposite samples, the main diffraction peak at $q \approx 0.040-0.043$ Å^{-1} was preserved across all sample types, although no additional peaks were detected (Figure 8C). A slight peak shift to higher q values can be seen in the hexagonally ordered fibrillar nanocomposites, likely originating from the drying-induced shrinkage in micellar dimensions under a vacuum during the measurement. A reduction in peak intensity and peak broadening was also observed for all cross-linked samples, possibly reflecting a distortion of the LLC structures and broadening of the micellar size distribution upon cross-linking. While it is challenging to determine whether the original structure is fully retained due to the absence of additional reflections or how the CNTs affect it, such observations are not uncommon. Previous studies of similar micellar cubic and hexagonally ordered Pluronic-based LLC systems have reported that higher-order reflections often disappear after cross-linking.[23,25,39]

3.5. Electrical Conductivity

The electrical conductivity of the CNT-Pluronic F127 nanocomposites is primarily influenced by the LLC phase of the material with the Fib exhibiting higher conductivity than that of the Mic samples (Figure 9B). Comparison with the materials' swelling behavior reveals a positive correlation, indicating that the electrical conductivity is mostly governed by water content, as anticipated (Figure 9A). In general, Fib samples absorbed more water due to the higher net mass of DA-F127 (as compared to the Mic samples), promoting swelling and correspondingly higher conductivity. The presence of CNTs affects the materials' swelling, particularly in the Fib hydrogels, where they reduce water uptake, leading to a slight decrease in conductivity. The reduced water uptake caused by the presence of CNTs is likely because they occupy polar functional groups of DA-F127, causing them to bind less water. Interestingly, even though Mic_HO is found to exhibit the lowest water uptake, it is found to be the most conductive among Mic samples. This phenomenon can be explained by the surface chemistry of the HO carbon nanotubes, which are well dispersed in the micellar cubic phase. Based on our previous study, HO CNTs are rich in oxygen atoms (around 16%) with around 30% of carbon atoms connected to oxygen via double bonds, some within carboxyl functional groups.[27] Such groups can reduce the pH and conductivity of water. In contrast, HNH carbon nanotubes have amide functional groups, which have a much weaker influence on the H^+ concentration. Hence, even though HNH-modified samples absorb more water, their electrical conductivity does not exceed that of the HO-modified samples. Overall, all the materials demonstrate comparable conductivity.

https://doi.org/10.1021/acsanm.6c00241
ACS Appl. Nano Mater. 2026, 9, 6665−6678

3.6. Drug Delivery

To investigate the drug delivery capacity of the selected nanocomposites, two model drugs were chosen, i.e., vancomycin (VCM) and ibuprofen (IBU). VCM is a polar glycopeptide antibiotic used as a last-resort treatment of Gram-positive bacterial infections, whereas IBU is an apolar nonsteroidal anti-inflammatory drug commonly used for the treatment of pain and inflammation. With water solubilities of 50 and 0.011 mg/mL for the VCM and IBU, respectively, the selected drugs have been previously used as models for the drug encapsulation and delivery from various delivery systems, including those based on Pluronic F127.[40−43] In this study, the as-prepared nanocomposite samples were loaded with the respective drugs using a postloading method in which dried samples were swollen in drug solution. Drug release was subsequently monitored in water or SDS for the VCM- or IBU-loaded samples, respectively.

For both Mic and Fib samples postloaded with VCM (Figure 9C), all samples displayed a substantially more uniform drug release compared to the IBU-loaded counterparts. Among the different Mic samples, nonsignificant differences in the drug release behavior were observed, indicating a limited impact of the CNT loading. Nevertheless, Mic_HO displayed a slightly higher cumulative drug release over approximately 20 h compared to the CNT-free Mic and Mic_HNH samples. As for the Fib samples, a higher overall amount of VCM was released, as compared to the Mic counterparts, which is potentially due to the increase in the relative DA-F127 amount in the sample (30 vs 35 wt %) and preferential localization of polar VCM within the polar domains of the Fib structure. Similar to the Mic samples, the introduction of different CNTs did not contribute to the uptake and release rate of the VCM with all samples plateauing at approximately 10−20 h.

For the IBU postloaded Mic and Fib samples (Figure 9D), drug release was generally lower and accompanied by large statistical variability, which is typical for the release of apolar drugs, potentially caused by the difficulties in establishing solubility equilibrium in the initial release stages. The CNT-free Mic sample displayed the highest drug release cumulatively, potentially indicating that introduction of the hydrophilic HO and HNH CNTs results in hindered IBU uptake due to the contrasting polarities. The CNT-free Fib sample exhibited the highest cumulative IBU release from the different Fib samples with the release pattern mirroring the different Mic samples. However, a clear trend was evident with both Fib_HO and Fib_HNH samples displaying the lowest IBU release, supporting the hypothesis that the presence of the hydrophilic HO and HNH CNTs potentially hinders the loading of the apolar IBU in the nanocomposite structure.

The drug delivery data indicate that the delivery from both the reference Mic and Fib systems as well as the HO and HNH containing nanocomposites follow previously established trends, where the VCM remains localized in the hydrophilic exterior of the micellar structure, whereas IBU is preferentially loaded into the hydrophobic micellar interior, resulting in reduced uptake and release.[42] Overall, apart from minor differences in the Mic samples, HO and HNH do not significantly contribute to the delivery of polar VCM. On the contrary, the IBU uptake and release seem to be significantly reduced for the Fib samples upon introduction of the CNTs.

The most likely explanation for the overall limited impact of CNTs on the drug delivery performance is the fact that the drugs were postloaded into already preformed hydrogels. In such cases, the CNT surface may already be embedded within the polymer matrix, prohibiting any direct drug−CNT interaction that could potentially contribute to increased loading and a more sustained delivery pattern. To test this hypothesis, a proof-of-concept experiment was conducted using the Mic samples, where the different CNTs were preloaded with VCM prior to the nanocomposite preparation. As evident from the drug release data (Figure 9C, inset), the presence of CNTs resulted in an approximately 30% increase in cumulative VCM release for both Mic_HO and Mic_HNH compared to the CNT-free Mic reference. This suggests that CNTs may contribute to better retention of the drug during the hydrogel formation. Notably, when comparing the preloaded samples with the postloaded ones, a substantially higher cumulative drug release was observed with about 100% increase for the CNT-free Mic sample (from ∼40 mg/g for postloaded samples to ∼80 mg/g for preloaded samples) and nearly 190% increase for both Mic_HO and Mic_HNH (from ∼40 mg/g for postloaded samples to ∼115 mg/g for preloaded samples). These preliminary results highlight the crucial role of sample preparation in maximizing the functional properties of CNT nanofillers in polymer nanocomposites and warrant further investigation.

4. CONCLUSIONS

In this study, the effects of chemically functionalized carbon nanotubes (CNTs) on the physicochemical and functional properties of uncross-linked and cross-linked lyotropic liquid crystalline (LLC) nanocomposites based on diacrylated Pluronic F127 were examined. The addition of oxidized (HO) and amidized (HNH) CNTs introduced phase-specific interactions within micellar cubic (Mic) and hexagonally ordered fibrillar (Fib) phases, affecting CNT dispersion, structural organization, and material processability via 3D printing. Among all formulations, Fib_HNH exhibited the most homogeneous CNT distribution, followed by Mic_HO, whereas Fib_HO and Mic_HNH showed poorer dispersion quality. In Fib_HO, the HOs likely caused local distortions of the structural arrangement of Pluronic-based LLCs, yielding gels with reduced viscosity and cross-linked samples that were slightly more thermally fragile (as evidenced by TEM and DSC analyses) yet displayed regions of visually increased local structural organization (as evidenced by SEM).

This study shows that incorporating CNTs into the DA-F127 nanocomposites is nontrivial and that both the solvent type and CNT surface chemistry critically influence structural and functional properties. Collectively, the results provide valuable guidelines for the informed design of a new class of nanocomposites. As demonstrated by performance studies, these nanocomposites hold promise as patient-specific and wound-specific hydrogel biomaterials aimed at filling complex defects, creating a wet environment favorable for healing, and delivering therapeutic agents locally. Combining drugs with CNTs during the material's synthesis enhanced drug retention within the hydrogel's matrix, resulting in higher loading and more sustained release. Postsynthesis soaking of drug was less effective but also yielded encouraging outcomes, particularly for polar drugs loaded in both Mic or Fib phases and for apolar drugs loaded in the Mic phase. Because different Pluronic-based LLCs are characterized by different mechanical and swelling properties, they can be tailored for specific applications. Beyond biomedical uses, these amphiphilic

https://doi.org/10.1021/acsanm.6c00241
ACS Appl. Nano Mater. 2026, 9, 6665−6678

CNT−hydrogel nanocomposites could also be explored for environmental remediation, especially wastewater treatment, where their dual affinity for polar and apolar species may enable effective pollutant capture. Further research should focus on deepening our understanding of CNT−polymer interactions and optimizing the material design for specific biomedical and technological applications.

■ ASSOCIATED CONTENT

Supporting Information

The Supporting Information is available free of charge at https://pubs.acs.org/doi/10.1021/acsanm.6c00241.

Additional images of the samples (macroscopic and microscopic), FTIR spectra, DSC curves, and SAXS peaks (PDF)

■ AUTHOR INFORMATION

Corresponding Author

Aleksandra Benko − *AGH University of Krakow, Faculty of Materials Science and Ceramics, 30-059 Krakow, Poland;* orcid.org/0000-0001-7474-3374; Email: abenko@agh.edu.pl

Authors

Annija Stepulane − *Department of Chemistry and Chemical Engineering, Chalmers University of Technology, Gothenburg SE-412 96, Sweden;* orcid.org/0000-0002-2974-2118

Marcel Zambrzycki − *AGH University of Krakow, Faculty of Materials Science and Ceramics, 30-059 Krakow, Poland;* orcid.org/0000-0002-7941-426X

Marta Gajewska − *AGH University of Krakow, Academic Centre for Materials and Nanotechnology, 30-059 Krakow, Poland;* orcid.org/0000-0003-3303-3768

Magdalena Ziąbka − *AGH University of Krakow, Faculty of Materials Science and Ceramics, 30-059 Krakow, Poland;* orcid.org/0000-0003-0702-7137

Martin Andersson − *Department of Chemistry and Chemical Engineering, Chalmers University of Technology, Gothenburg SE-412 96, Sweden;* orcid.org/0000-0003-1523-4697

Complete contact information is available at: https://pubs.acs.org/10.1021/acsanm.6c00241

Notes

The authors declare no competing financial interest.

■ ACKNOWLEDGMENTS

This study has been supported by the program "Excellence initiative - research university" for the AGH University of Krakow (Grant ID 4862; PI: A. Benko) and by the National Centre for Research and Development under grant no. LIDER/7/0020/L-11/19/NCBR/2020 (PI: A. Benko). The research was supported by the Area of Advance in Materials Science at Chalmers University of Technology and by the Knut and Alice Wallenberg Foundation through the Wallenberg Academy Fellows program. Experimental work was partly conducted at the Chalmers Materials Analysis Laboratory (CMAL). The authors would like to thank Amferia AB for providing the DA-F127 used in this study.

■ REFERENCES

(1) Teixeira-Santos, R.; Gomes, M.; Gomes, L. C.; Mergulhão, F. J. Antimicrobial and anti-adhesive properties of carbon nanotube-based surfaces for medical applications: a systematic review. *iScience* **2021**, *24* (1), No. 102001.

(2) Benko, A.; Medina-Cruz, D.; Vernet-Crua, A.; O'Connell, C. P.; Święt ek, M.; Barabadi, H.; Saravanan, M.; Webster, T. J. Nanocarrier drug resistant tumor interactions: novel approaches to fight drug resistance in cancer. *Cancer Drug Resist.* **2021**, *4* (2), 264−297.

(3) Balandin, A. A. Thermal properties of graphene and nanostructured carbon materials. *Nat. Mater.* **2011**, *10* (8), 569−581.

(4) Ebbesen, T. W.; Lezec, H. J.; Hiura, H.; Bennett, J. W.; Ghaemi, H. F.; Thio, T. Electrical conductivity of individual carbon nanotubes. *Nature* **1996**, *382* (6586), 54−56.

(5) Kostarelos, K.; Bianco, A.; Prato, M. Promises, facts and challenges for carbon nanotubes in imaging and therapeutics. *Nat. Nanotechnol* **2009**, *4* (10), 627−633.

(6) Benko, A.; Medina-Cruz, D.; Wilk, S.; Ziąbka, M.; Zagrajczuk, B.; Menaszek, E.; Barczyk-Woźnicka, O.; Guisbiers, G.; Webster, T. J. Anticancer and antibacterial properties of carbon nanotubes are governed by their functional groups. *Nanoscale* **2023**, *15* (45), 18265−18282.

(7) Kostarelos, K. The long and short of carbon nanotube toxicity. *Nat. Biotechnol.* **2008**, *26* (7), 774−776.

(8) Kostarelos, K.; Lacerda, L.; Pastorin, G.; Wu, W.; Wieckowski, S.; Luangsivilay, J.; Godefroy, S.; Pantarotto, D.; Briand, J.-P.; Muller, S.; Prato, M.; Bianco, A. Cellular uptake of functionalized carbon nanotubes is independent of functional group and cell type. *Nat. Nanotechnol* **2007**, *2* (2), 108−113.

(9) Van den Broeck, L.; Piluso, S.; Soultan, A. H.; De Volder, M.; Patterson, J. Cytocompatible carbon nanotube reinforced polyethylene glycol composite hydrogels for tissue engineering. *Mater. Sci. Eng., C* **2019**, *98*, 1133−1144.

(10) Zhijiang, C.; Cong, Z.; Jie, G.; Qing, Z.; Kongyin, Z. Electrospun carboxyl multi-walled carbon nanotubes grafted polyhydroxybutyrate composite nanofibers membrane scaffolds: Preparation, characterization and cytocompatibility. *Mater. Sci. Eng., C* **2018**, *82*, 29−40.

(11) Wilk, S.; Medina-Cruz, D.; Zambrzycki, M.; Szewczyk, P. K.; Nocuń, M.; Menaszek, E.; Webster, T. J.; Benko, A. The addition of carbon nanotubes modifies the biological, physicochemical, and electrical properties of carbon nanofiber composites. *Chem. Eng. J.* **2023**, *455*, No. 140617.

(12) Spitalsky, Z.; Tasis, D.; Papagelis, K.; Galiotis, C. Carbon nanotube−polymer composites: Chemistry, processing, mechanical and electrical properties. *Prog. Polym. Sci.* **2010**, *35* (3), 357−401.

(13) Lee, S.-J.; Zhu, W.; Nowicki, M.; Lee, G.; Heo, D. N.; Kim, J.; Zuo, Y. Y.; Zhang, L. G. 3D printing nano conductive multi-walled carbon nanotube scaffolds for nerve regeneration. *J. Neural Eng.* **2018**, *15* (1), No. 016018.

(14) Merck. TissueFab bioink Conductive; https://www.merckmillipore.com/GE/en/product/aldrich/926078, https://www.sigmaaldrich.com/PL/pl/product/aldrich/915726. (accessed April 7, 2026).

(15) Alpatova, A. L.; Shan, W.; Babica, P.; Upham, B. L.; Rogensues, A. R.; Masten, S. J.; Drown, E.; Mohanty, A. K.; Alocilja, E. C.; Tarabara, V. V. Single-walled carbon nanotubes dispersed in aqueous media via non-covalent functionalization: Effect of dispersant on the stability, cytotoxicity, and epigenetic toxicity of nanotube suspensions. *Water Res.* **2010**, *44* (2), 505−520.

(16) Liu, C.-X.; Choi, J.-W. Improved Dispersion of Carbon Nanotubes in Polymers at High Concentrations. *Nanomaterials* **2012**, *2* (4), 329−347.

(17) Sun, Z.; Yin, Z.; Zhang, M.; Guo, D.; Ran, F. Poloxamer 407 Combined with Polyvinylpyrrolidone To Prepare a High-Performance Poly(ether sulfone) Ultrafiltration Membrane. *ACS Omega* **2023**, *8* (42), 39783−39795.

(18) Święt ek, M.; Tokarz, W.; Benko, A.; Nocuń, M.; Mázl-Chánová, E.; Błażewicz, M. Fabrication of CNT/ION hybrids and their impact

on the biomedical applicability of PCL-based composite films. *Polym. Compos* **2019**, *40* (S2), E1818−E1830.
(19) Holmqvist, P.; Alexandridis, P.; Lindman, B. Phase Behavior and Structure of Ternary Amphiphilic Block Copolymer−Alkanol−Water Systems: Comparison of Poly(ethylene oxide)/Poly(propylene oxide) to Poly(ethylene oxide)/Poly(tetrahydrofuran) Copolymers. *Langmuir* **1997**, *13* (9), 2471−2479.
(20) Holmqvist, P.; Alexandridis, P.; Lindman, B. Modification of the Microstructure in Poloxamer Block Copolymer−Water−"Oil" Systems by Varying the "Oil" Type. *Macromolecules* **1997**, *30* (22), 6788−6797.
(21) Nie, S.; Hsiao, W. L.; Pan, W.; Yang, Z. Thermoreversible Pluronic F127-based hydrogel containing liposomes for the controlled delivery of paclitaxel: in vitro drug release, cell cytotoxicity, and uptake studies. *Int. J. Nanomedicine* **2011**, *6*, 151−166.
(22) Lee, S. H.; Lee, J. E.; Baek, W. Y.; Lim, J. O. Regional delivery of vancomycin using pluronic F-127 to inhibit methicillin resistant Staphylococcus aureus (MRSA) growth in chronic otitis media in vitro and in vivo. *J. Controlled Release* **2004**, *96* (1), 1−7.
(23) He, W. X.; Rajasekharan, A. K.; Tehrani-Bagha, A. R.; Andersson, M. Mesoscopically ordered bone-mimetic nanocomposites. *Adv. Mater.* **2015**, *27* (13), 2260−4.
(24) Rajasekharan, A. K.; Andersson, M. Role of Nanoscale Confinement on Calcium Phosphate Formation at High Supersaturation. *Cryst. Growth Des* **2015**, *15* (6), 2775−2780.
(25) Stepulane, A.; Ahlgren, K.; Rodriguez-Palomo, A.; Rajasekharan, A. K.; Andersson, M. Lyotropic liquid crystal elastomers for drug delivery. *Colloids Surf. B Biointerfaces* **2023**, *226*, No. 113304.
(26) Atefyekta, S.; Blomstrand, E.; Rajasekharan, A. K.; Svensson, S.; Trobos, M.; Hong, J.; Webster, T. J.; Thomsen, P.; Andersson, M. Antimicrobial Peptide-Functionalized Mesoporous Hydrogels. *ACS Biomater Sci. Eng.* **2021**, *7* (4), 1693−1702.
(27) Benko, A.; Duch, J.; Gajewska, M.; Marzec, M.; Bernasik, A.; Nocuń, M.; Piskorz, W.; Kotarba, A. Covalently bonded surface functional groups on carbon nanotubes: from molecular modeling to practical applications. *Nanoscale* **2021**, *13* (22), 10152−10166.
(28) Benko, A.; Medina-Cruz, D.; Duch, J.; Popiela, T.; Wilk, S.; Bińczak, M.; Nocuń, M.; Menaszek, E.; Geoffrion, L. D.; Guisbiers, G.; Kotarba, A.; Webster, T. J. Conductive all-carbon nanotube layers: Results on attractive physicochemical, anti-bacterial, anticancer and biocompatibility properties. *Mater. Sci. Eng., C* **2021**, *120*, No. 111703.
(29) Holmqvist, P.; Alexandridis, P.; Lindman, B. Modification of the Microstructure in Block Copolymer−Water−"Oil" Systems by Varying the Copolymer Composition and the "Oil" Type: Small-Angle X-ray Scattering and Deuterium-NMR Investigation. *J. Phys. Chem. B* **1998**, *102* (7), 1149−1158.
(30) Konuray, O.; Fernández-Francos, X.; Ramis, X.; Serra, À. State of the Art in Dual-Curing Acrylate Systems. *Polymers* **2018**, *10* (2), 178.
(31) Wu, Y. L.; Sprik, R.; Poon, W. C. K.; Eiser, E. Effect of salt on the phase behaviour of F68 triblock PEO/PPO/PEO copolymer. *J. Phys: Condens Matter* **2006**, *18* (19), 4461.
(32) Yan, B.; Zhou, H.; Lai, J.; Wang, Z.; Luo, C.; Liu, H.; Jin, X.; Ma, A.; Chen, W. Pluronic F127 gels fabricated by thiol−ene click chemistry: preparation, gelation dynamics, swelling behaviors and mechanical properties. *Polym. Bull.* **2019**, *76* (12), 6049−6061.
(33) Moreno, S.; Voit, B.; Gaitzsch, J. The chemistry of cross-linked polymeric vesicles and their functionalization towards biocatalytic nanoreactors. *Colloid Polym. Sci.* **2021**, *299* (3), 309−324.
(34) Shriky, B.; Vigato, A. A.; Sepulveda, A. F.; Machado, I. P.; de Araujo, D. R. Poloxamer-based nanogels as delivery systems: how structural requirements can drive their biological performance? *Biophys Rev.* **2023**, *15* (4), 475−496.
(35) Smith, B. C. The C═O Bond, Part VI: Esters and the Rule of Three; https://www.spectroscopyonline.com/view/co-bond-part-vi-esters-and-rule-three (accessed 05.09.2024).
(36) Sichina, W. J. *Measurement of Tg by DSC, Application note*; Perkin Elmer Instruments, 2000; pp 1−5.
(37) Batool, N.; Mahmood, A.; Sarfraz, R. M.; Ijaz, H.; Zafar, N.; Hussain, Z. Formulation and evaluation of interpenetrating polymeric network for controlled drug delivery. *Drug Dev. Ind. Pharm.* **2021**, *47* (6), 931−946.
(38) Naeimi, M.; Tajedin, R.; Farahmandfar, F.; Naeimi, M.; Monajjemi, M. Preparation and characterization of vancomycin-loaded chitosan/PVA/PEG hydrogels for wound dressing. *Mater. Res. Express* **2020**, *7* (9), No. 095401.
(39) Rajasekharan, A. K.; Gyllensten, C.; Blomstrand, E.; Liebi, M.; Andersson, M. Tough Ordered Mesoporous Elastomeric Biomaterials Formed at Ambient Conditions. *ACS Nano* **2020**, *14* (1), 241−254.
(40) Almeida, H.; Lobão, P.; Frigerio, C.; Fonseca, J.; Silva, R.; Sousa Lobo, J. M.; Amaral, M. H. Preparation, characterization and biocompatibility studies of thermoresponsive eyedrops based on the combination of nanostructured lipid carriers (NLC) and the polymer Pluronic F-127 for controlled delivery of ibuprofen. *Pharm. Dev Technol.* **2017**, *22* (3), 336−349.
(41) Veyries, M. L.; Couarraze, G.; Geiger, S.; Agnely, F.; Massias, L.; Kunzli, B.; Faurisson, F.; Rouveix, B. Controlled release of vancomycin from Poloxamer 407 gels. *Int. J. Pharm.* **1999**, *192* (2), 183−193.
(42) Stepulane, A.; Rajasekharan, A. K.; Andersson, M. Multifunctional Surface Modification of PDMS for Antibacterial Contact Killing and Drug-Delivery of Polar, Nonpolar, and Amphiphilic Drugs. *ACS Appl. BioMater.* **2022**, *5* (11), 5289−5301.
(43) Rai, A.; Senapati, S.; Saraf, S. K.; Maiti, P. Biodegradable poly(ε-caprolactone) as a controlled drug delivery vehicle of vancomycin for the treatment of MRSA infection. *J. Mater. Chem. B* **2016**, *4* (30), 5151−5160.

https://doi.org/10.1021/acsanm.6c00241
ACS Appl. Nano Mater. 2026, 9, 6665−6678